Advanced Parametric Lobe Mixer Concepts for Internally Mixed Nozzles

William V. Banks*

HX5, LLC, Brook Park, OH, 44142, USA

A continuation of efforts to optimize a dual-stream lobe mixer for supersonic commercial flight is detailed, adding scarfing and scalloping features to a baseline lobe mixer previously optimized within a baseline parametric space. These "advanced features" are parameterized by four quantities: scarfing angle ζ, scallop height h_s, scallop depth d_s, and scallop conic focal parameter ρ_s. Two baseline mixers, one parallel and one vortical, form the basis for an eighteen-case study to investigate the effects of each parameter in single-axis fashion. Aerodynamic performance is evaluated through velocity coefficient C_V. Moderate performance increases are seen with increasing scallop height and depth on the parallel mixer, and with increasing scarfing angle on the vortical mixer. Flowfield analysis is presented through visualization of axial and cross-stream vorticity development through the duct, as well as density variation. A correlation between axial vorticity and density variation decay was found, with earlier introduction of axial vorticity found to result in improved aerodynamic performance and potential noise suppression.

Nomenclature

A	=	area
AR	=	area ratio A_b/A_c
BPR	=	bypass ratio $\dot{m}_b/\dot{m}_c$
c	=	polynomial coefficient
C_V	=	nozzle velocity coefficient F_g/F_{g_i}
d_s	=	normalized scallop depth
ER	=	extraction ratio NPR_b/NPR_c
F_g	=	nozzle net thrust
h_s	=	scallop height
L	=	length
M	=	Mach number
$\dot{m}$	=	mass flow
n	=	mixer lobe count
NTR	=	nozzle temperature ratio T_t/T_∞
NPR	=	nozzle pressure ratio $p_{t,IN}/p_\infty$
p	=	pressure OR point location
r	=	radius
R	=	specific gas constant for air
Re	=	Reynolds number
t	=	cowl thickness
T	=	temperature
TKE	=	turbulent kinetic energy
v	=	velocity
y^+	=	non-dimensionalized wall distance
γ	=	ratio of specific heats
ζ	=	scarfing angle
η	=	lobe bias coefficient
θ	=	azimuthal coordinate OR angle
ρ	=	density

---
*Aerospace Engineer, NASA GRC Propulsion Division, Inlets and Nozzles Branch, AIAA Member

ρ_s	=	scallop conic focal parameter
σ_ρ	=	density standard deviation
ϕ	=	lobe penetration fraction
ω	=	vorticity
∂_{TE}	=	mixer trailing edge slope

Subscripts

6	=	nozzle inflow plane
7	=	nozzle converging section inflow plane
8	=	nozzle throat plane
9	=	nozzle exit plane
b	=	bypass
c	=	core
C	=	converging section
i	=	ideal
IN	=	inflow
M	=	mixer section
n	=	nacelle OR cowl
p	=	plug
pk	=	peak
ptr	=	plug truncation
S	=	plug shaft section
t	=	total
T	=	turbine rear frame tailcone section
tr	=	trough
∞	=	freestream

I. Introduction

As part of NASA's ongoing Commercial Supersonic Technology (CST) project, a focused research effort is underway to mitigate airport noise from supersonic vehicles, with an emphasis on using physics-based models to reduce noise prediction uncertainty. This requires the expansion of NASA's empirical model databases to include supersonic components for near-term applications. While external industry designs can be leveraged for some components, there is a lack of data openly available for commercial supersonic nozzle systems. Fortunately, NASA is no stranger to the design of these systems. In 1990, Stitt [1] published a compendium of NASA's experience developing nozzle systems following the Supersonic Transport (SST) and Supersonic Cruise Research (SCR) projects carried out from 1963-1985. Several key points with relevance to the current study were laid forth:

- 1% decrease in nozzle performance translates to roughly 8% decrease in payload capacity
- Commercial supersonic vehicles are uniquely sensitive to variable A_8/A_9 requirements through the mission profile
- Plug nozzles provide the best thrust and noise benefits, have reduced complexity and leakage than other variable-area nozzle types, and minimize boattail drag

Zaman and Heberling [2] laid out CFD predictions and preliminary test results for various single-stream plug nozzle configurations with the goal of informing NASA's nozzle system design. Additionally, they presented a large literature review affirming the selection of the plug nozzle over other nozzle designs. Efforts in the literature have laid a solid foundation for an understanding of turbojet nozzle systems, but modern noise regulations and range requirements warrant a turbofan engine. For a plug nozzle to be most effective, bypass and core streams should be mixed prior to the start of duct convergence to a throat section. Since commercial aircraft viability is highly sensitive to nozzle performance at the supersonic cruise point, any nozzle system considered for noise reduction at takeoff must include a mixing apparatus optimized for thrust performance at supersonic cruise.

One strategy to accelerate the mixing process is lobe scalloping. Merati and Cooper [3] experimentally compared lobed mixers to scalloped mixers in a dual-stream, internal water duct. They found the introduction of scallops generated

an additional small-scale streamwise vortex pair along the shear layer between streams, as well as increased turbulence intensity. Both of these flow mechanisms are known to contribute to mixing effectiveness, but with the penalty of induced total pressure loss.

The current work is part of a larger research effort to provide industry with design tools and guidance to minimize jet noise while maintaining aerodynamic performance and efficiency. In a precursor paper by Banks [4], five basic geometric parameters were identified to define a basic internal lobe mixer, with an automated toolset showcased to rapidly build and mesh nozzle geometries from these parameters. The simple sinusoidally-deformed lobe mixer design was shown to be effective at improving mixing performance in a dual-stream nozzle with a long, constant-area mixing duct. A design-of-experiments (DoE) study was performed to create a reduced-order surrogate model for performance optimization. Several conclusions were drawn from the study results:

- Mixer lobe penetration ϕ had a less-than-expected impact on performance, and an optimum value for ϕ was seen around 50-55%
- Mixer trailing edge slope ∂_{TE} had a large impact on performance, increasing velocity coefficient C_V without introducing excessive pressure losses
- Ineffective mixers resulted in streams remaining independent, while overly aggressive mixers caused flow separation
- Strong axial vorticity ω_x development through the duct typically correlated to high mixer performance

Expanding on these basic lobe mixer parameters, four additional parameters were investigated that add scarfing and lobe scallops to the mixers in various configurations. These advanced features are intended to introduce the shear layer earlier in the duct and enhance streamwise vorticity in order to boost mixer performance with minimal induced total pressure loss. The toolset introduced in Banks [4] was expanded to include these parameters in automated builds. A collection of mixer geometries generated with this toolset were analyzed via RANS CFD using NASA's FUN3D code. Interrogation of the numerically-generated flowfields provides insight into how the addition of the advanced features contributes to flow mixing and potentially improves nozzle performance, both aerodynamically and acoustically.

II. Methodology

A. Study Environment

A 55-tonne Supersonic Transport Concept Aeroplane (STCA) has been developed at NASA by Berton et al. [5] to support consideration of new environmental standards for commercial supersonic vehicles. To date, this notional supersonic business jet has been used in several studies within the CST framework, providing reference mission conditions for analytical studies. Simulation boundary conditions for the current work, listed in Table 1, were defined based on the supersonic cruise mission point for a single engine of the tri-jet 55t STCA. Quasi-1D analysis predicts $\dot{m}$ = 146.2 lbm/s and bypass ratio (BPR) = 3.33 for the listed conditions. While the airport noise effort is chiefly concerned with reducing noise at takeoff, nozzle performance is most impactful at supersonic cruise.

Table 1   Key STCA supersonic cruise conditions.

Property	Value
p_∞	1.68 lb/in^2
T_∞	217 K
M_∞	1.4
NPR$_b$	6.158
NPR$_c$	5.633
NTR$_b$	1.736
NTR$_c$	4.654

As part of the effort to provide noise reduction tools to the burgeoning commercial supersonics industry, a nozzle design toolkit called Supersonic Parametric Nozzle Design (SPAND) is in development. Currently, it takes inputs in the form of a python dictionary namelist file of geometric parameters and returns the desired nozzle geometry components as either a 3D point file, an .iges database file, or a Pointwise database file. Additionally, SPAND can generate an unstructured tetrahedral volume grid in Pointwise and output for use with a three-dimensional unstructured CFD solver, such as NASA's FUN3D. A plug nozzle can be generated for single-stream or dual-stream inflows, with throat and exit areas determined by inflow Nozzle Pressure Ratios (NPRs). Dual-stream nozzles can be specified as either confluent or force-mixed, returning a nozzle with an axisymmetric splitter or lobed mixer, respectively. Scarfing and scalloping can be added to a lobe mixer via axisymmetric cutout.

A plug centerbody and nozzle cowl were designed to house the various mixer configurations considered. Dimensions were selected to adhere to STCA conditions, with exit area sized for ideal expansion at supersonic cruise conditions. The nozzle centerbody was contoured to model expected engine geometry, with extra length added to the straight section to facilitate flow mixing analysis. Key nozzle dimensions, shown in Table 2, along with NPR values, were plugged into SPAND as inputs. The resulting axisymmetric cross-section is shown in Fig. 1 with a confluent axisymmetric splitter inserted for reference. The target extraction ratio (ER) and BPR were taken from the STCA analysis, and area ratio (AR) was iteratively selected to ensure the input ER produced the desired confluent BPR.

Table 2   Key nozzle dimensions.

Dimension	Value	Dimension	Value
$r_{ic,6}$	11.5 in	t_6	3.75 in
$r_{ob,6}$	25.75 in	t_9	0.125 in
$r_{ic,7}$	8 in	θ_P	15°
$r_{ob,7}$	25.75 in	L_T	20 in
$r_{ic,7}$	8 in	L_S	20 in
r_8	20.351 in	L_C	30 in
r_n	25.75 in	x_{IP}^*	0.4
r_c	20.351 in	r_{ptr}	0.2 in
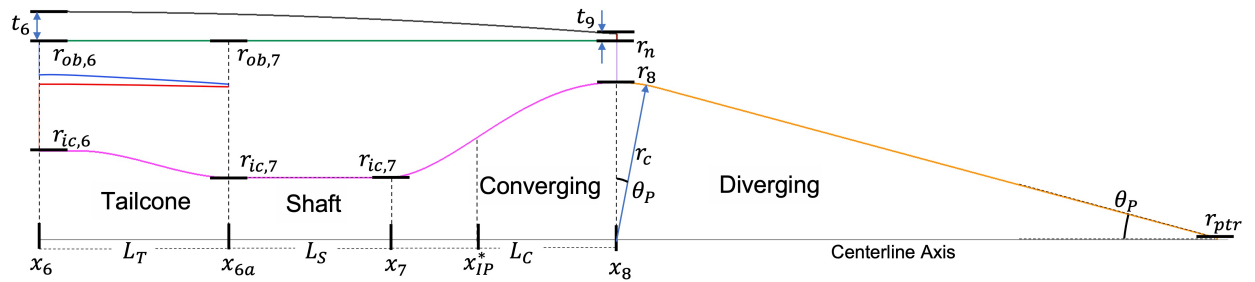
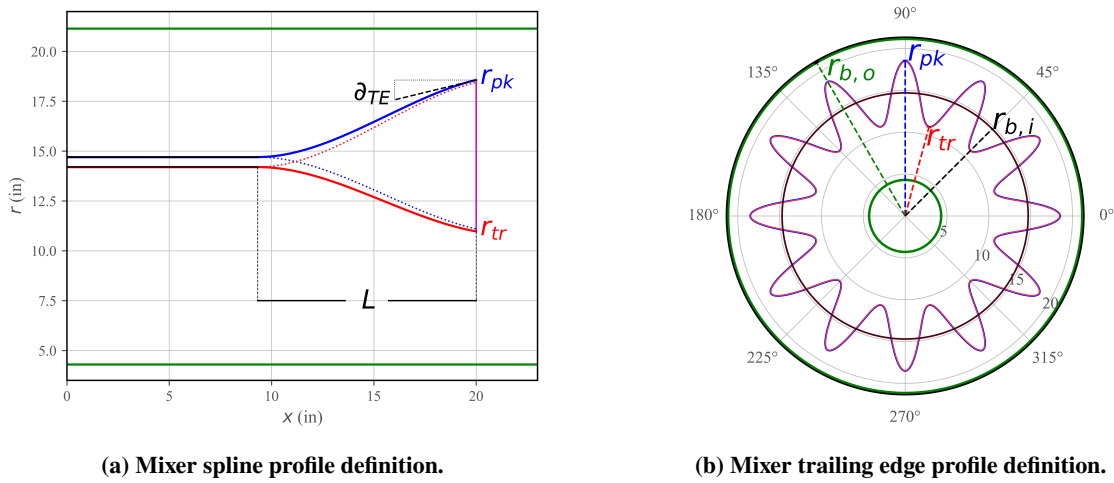**Fig. 1   Axisymmetric cross-section of study housing nozzle.**

B. Baseline Mixer Construction

Mixer construction in SPAND begins by generating a grid of points in three-dimensional Cartesian coordinates using the procedure described in the precursor study [4] and illustrated in Fig 2. For this work, the theta domain is discretized using a specified number of points, and an individual Cartesian-point spline curve is exported at each theta value for both bypass and core surfaces. Root and trailing edge curves for each surface are also exported. These curves are imported to Pointwise, and B-spline surface panels are generated along each theta value using the spline curves as bounds. Surface grids are then constructed to model the mixer surfaces using these panels as the underlying databases.
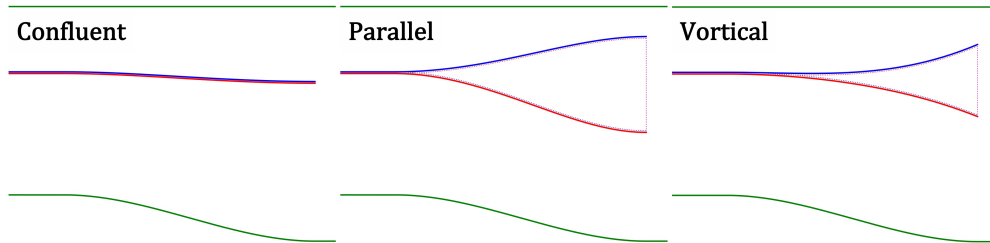
4

Two baseline lobed mixers were defined using the parameters shown in Table 3, illustrated against a confluent splitter in Fig. 3 The parallel mixer relies on a larger flowstream penetration to create more shear layer surface area with minimal flow turning to reduce loss. The vortical mixer uses an outward-angled trailing edge to maintain mixing performance while minimizing flowstream penetration, at the expense of generating additional secondary flows.

Table 3   Baseline mixer input parameters.

Parameter	Confluent	Parallel	Vortical
n	0	12	12
ϕ	0	60%	50%
L_M	0	0.8	0.8
η	0	0	-0.125
∂_{TE}	0	0	0.4

(a) Mixer spline profile definition.

(b) Mixer trailing edge profile definition.

Fig. 2   Basic lobe mixer two-dimensional profiles [4]

Fig. 3   Baseline mixer spline profiles compared to confluent splitter.

C. Advanced Feature Addition

Scarfing and scalloping cuts were axisymmetrically applied to both mixers using the four parameters described in Table 4. Figure 4 illustrates how the parameters relate to the geometry of the cutting curves generated by SPAND, with ζ defining the scarf cut and h_s, d_s, and ρ_s^* defining the scallop cut. Unlike the basic lobe mixer parameter space, the

scallop cut parameters are dependent on mixer and nozzle geometry to facilitate a robust design space that is consistently applicable to as many mixer/nozzle configurations as possible.

Table 4   Advanced mixer geometry design parameters.

Parameter	Symbol	Description
Scarf Angle	ζ	Axisymmetric angle at which the lobe mixer trailing edge is scarfed
Scallop Height	h_s	Scallop cutout height, as a fraction of mixer lobe height
Scallop Depth	d_s	Scallop cutout depth, as a fraction of mixer length
Focal Parameter	ρ_s^*	Corrected scallop cutout focal parameter
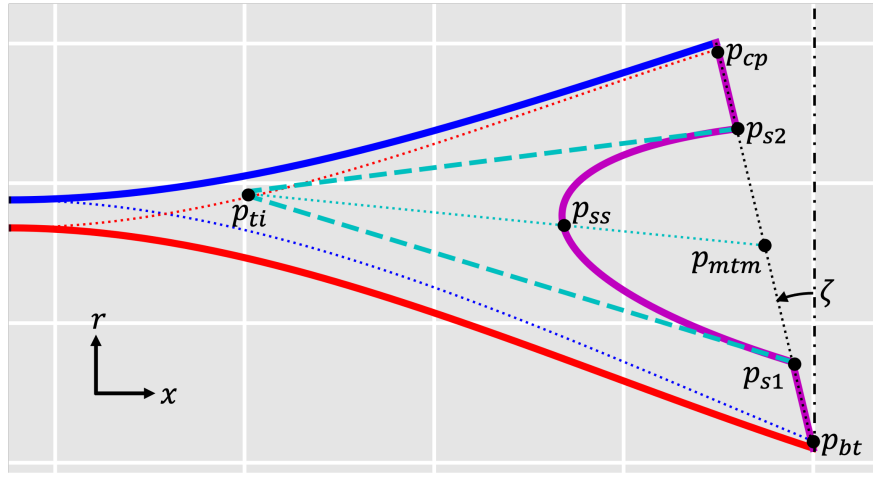
Fig. 4   Axisymmetric cross-section of study housing nozzle.

The scarf cut line is rotated by angle ζ about either the lobe trough, if positive (+), or the lobe peak, if negative (-). The resulting mixer trailing edge endpoints in the x-r plane are bypass trough $p_{bt} = (x_{bt}, r_{bt})$ and core peak $p_{cp} = (x_{cp}, r_{cp})$. The scallop curve is defined as a conic section in the x-r plane using the general form given in Eq. 1. Endpoints $p_{s1} = (x_{s1}, r_{s1})$ and $p_{s2} = (x_{s2}, r_{s2})$ are placed along the mixer trailing edge line such that Eqs. 2 and 3 are satisfied. The shoulder point $p_{ss} = (x_{ss}, r_{ss})$ is placed using the following steps:

- The mixer TE midpoint $p_{mtm} = (x_{mtm}, r_{mtm})$ is defined as $x_{mtm} = (x_{s2} - x_{s1})/2$ and $r_{mtm} = (r_{s2} - r_{s1})/2$
- The mixer root midpoint $p_{mrm} = (x_{mrm}, r_{mrm})$ is defined as $x_{mrm} = (x_{mrb} - x_{mrc})/2$ and $r_{mrm} = (r_{mrb} - r_{mrc})/2$
- p_{ss} is placed along the vector $p_{mtm} - p_{mrm}$ such that Eq. 4 is satisfied.

$$c_1 x^2 + c_2 xr + c_3 r^2 + c_4 x + c_5 r + 1 = 0 \tag{1}$$

$$|x_{s2} - x_{s1}| = h_s * |x_{bt} - x_{cp}| \quad ; \quad |r_{s2} - r_{s1}| = h_s * |r_{bt} - r_{cp}| \tag{2}$$

$$x_{cp} - x_{s2} = x_{s1} - x_{bt} \quad ; \quad r_{cp} - r_{s2} = r_{s1} - r_{bt} \tag{3}$$

$$x_{ss} = x_{mtm} - d_s(x_{mtm} - x_{mrm}) \quad ; \quad r_{ss} = r_{mtm} - d_s(r_{mtm} - r_{mrm}) \tag{4}$$

The range of the scallop conic focal parameter ρ_s is highly dependent on h_s and d_s, so a surrogate parameter ρ_s^* is defined to map the range of acceptable inputs through to [0,1]. This is done with the correction equation Eq. 5, where

$c_{\rho 1}$, $c_{\rho 2}$, and $c_{\rho 3}$ are empirical coefficients derived from geometric limits for each baseline mixer. The tangent intersect point $p_{ti} = (x_{ti}, r_{ti})$ is then extrapolated from the vector $p_{mtm} - p_{ss}$ such that Eq.6 is satisfied. Slopes at the endpoints are then found via the Eq.7. The general conic coefficients are then found from Eq. 8, and an axisymmetric cut curve is generated in the x-r plane between p_{s1} and p_{s2}. Though this method relies on dependent parameters, the result is a robust design system with a continuous and largely stable parametric range across a wide band of baseline mixer and nozzle configurations. This supports plug-and-play automated optimization for a variety of applications.

$$\rho_s = 1 - (1 - (c_{\rho 1}h_s^2 + c_{\rho 2}h_s + c_{\rho 3})\frac{d_s}{0.5}) * (1 - \rho_s^*) \tag{5}$$

$$x_{ti} = x_{mtm} - (x_{mtm} - x_{ss})/\rho_s \quad ; \quad r_{ti} = r_{mtm} - (r_{mtm} - r_{ss})/\rho_s \tag{6}$$

$$r'_{s1} = \frac{r_{s1} - r_{ti}}{x_{s1} - x_{ti}} \quad ; \quad r'_{s2} = \frac{r_{s2} - r_{ti}}{x_{s2} - x_{ti}} \tag{7}$$

$$\begin{bmatrix} x_{s1}^2 & x_{s1}r_{s1} & r_{s1}^2 & x_{s1} & r_{s1} \\ x_{s2}^2 & x_{s2}r_{s2} & r_{s2}^2 & x_{s2} & r_{s2} \\ x_{ss}^2 & x_{ss}r_{ss} & r_{ss}^2 & x_{ss} & r_{ss} \\ 2 * x_{s1} & r_{s1} + x_{s1}r'_{s1} & 2r_{s1}r'_{s1} & 1 & r'_{s1} \\ 2 * x_{s2} & r_{s2} + x_{s2}r'_{s2} & 2r_{s2}r'_{s2} & 1 & r'_{s2} \end{bmatrix} \begin{bmatrix} c_1 \\ c_2 \\ c_3 \\ c_4 \\ c_5 \end{bmatrix} = \begin{bmatrix} -1 \\ -1 \\ -1 \\ 0 \\ 0 \end{bmatrix} \tag{8}$$

D. Gridding

Pointwise v18.4 R2 was used to discretize the domains as three-dimensional unstructured grids. Each fluid domain was divided into interior and exterior blocks to enable controlled refinement and subdivide nozzle surfaces for thrust accounting. A cylindrical farfield was extended 10 nozzle exit diameter lengths from the centerline axis in the radial direction and 40 nozzle exit diameter lengths from the nozzle exit plane in the axial direction. Pointwise's T-Rex algorithm was used to resolve the boundary layers with anisotropic cells grown from the walls. In general, grid refinement was set through defined connector spacings, with key spacing values shown in Table 5. A grid convergence study with a similar gridding procedure concluded a grid convergence error of $\Delta C_V \pm 0.001$ should be implied going forward [4].

Table 5   Nozzle grid connector spacings.

Description	Spacing
Interior Baseline	0.2 $in.$
Exterior Baseline	0.5 $in.$
Mixer Trailing Edge	0.08 $in.$
Mixer Trailing Edge Thickness	0.0625 $in.$
Farfield	10 $in.$
T-Rex 1st Layer	$4e$-5 $in.$
T-Rex Growth Rate	1.3

Full grids ranged in size from 12M to 13M nodes. Near-wall y^+ values were typically seen to be between 0.1-0.15, with a maximum value of 0.97 occurring on the mixer trailing edge. Figure 5a shows surface boundary meshes for an example case, while Fig. 5b shows near-wall y^+ contours on the mixer bypass surface for the example case.
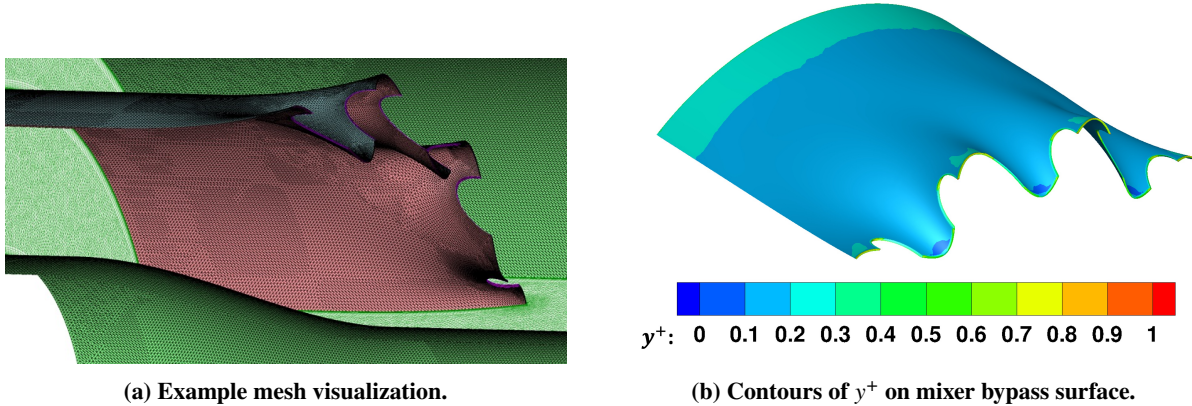
(a) Example mesh visualization.

y^+: 0 0.1 0.2 0.3 0.4 0.5 0.6 0.7 0.8 0.9 1

(b) Contours of y^+ on mixer bypass surface.

Fig. 5 Mesh visualization and y^+ values for an example nozzle.

E. Numerical Simulation

NASA's FUN3D code, perfect-gas v13.3, was used to solve the RANS equations, resolving turbulence with the two-equation shear stress transport turbulence model of Menter [6], with a vorticity source term modification. Flow is assumed to be fully turbulent. Two subsonic inlet boundaries with prescribed values for NPR and NTR were placed at the bypass and core stream inflow planes. Symmetry planes were defined at the x-y and x-z planes to model the full nozzle from the quarter-annular geometry. Solid surfaces were defined as adiabatic viscous walls and grouped by component to separate body forces for detailed thrust analysis. Freestream conditions reflected a supersonic cruise mission point profile, with $M_\infty = 1.4$, $Re_\infty = 5.4e6$, and $T_\infty = 217K$. Table 6 summarizes the boundary conditions imposed.

Table 6   Simulation boundary conditions.

Boundary	Type	FUN3D Code	NPR	NTR
Core Inflow	Subsonic Inflow	7011	5.534	4.654
Bypass Inflow	Subsonic Inflow	7011	6.268	1.736
x-z Symmetry	Symmetry_y	6662	–	–
x-y Symmetry	Symmetry_z	6663	–	–
Farfield Inflow	Freestream	5050	–	–
Farfield	Farfield	5000	–	–
Farfield Outflow	Extrapolate	5026	–	–
Nozzle Surfaces	Viscous Wall	4000	–	–

CFL numbers were set to ramp linearly over the first 1000 iterations, with convective CFL number ramping from 1 to 50 and turbulent CFL number ramping from 0.2 to 20. Additionally, the first 1000 iterations were run using a first-order accurate scheme, switching to second-order accuracy for the remainder of the simulation. No strict definition was set for convergence, but RANS equation residuals, total inlet mass flow ($\dot{m}_{IN}$), and C_V were all monitored to ensure a stable solution was achieved. Convergence was typically seen within 3000 iterations, and all simulations were run for at least 10000 total iterations. Simulations were performed on the NASA Advanced Supercomputing (NAS) platform using eight 28-core Broadwell nodes, for a total of 224 cores per case. Simulations typically ran to convergence in 6 hours, for a total of roughly 1350 CPU-hrs per case.

III. Results

The goal of this work was to demonstrate the scarfing and scalloping capabilities of the SPAND tool and briefly investigate the flow physics produced by different configurations. To this end, nine configurations were generated and analyzed for both the parallel and vortical baseline mixers, representing a 3-point study on each parameter introduced here as summarized in Table 7.
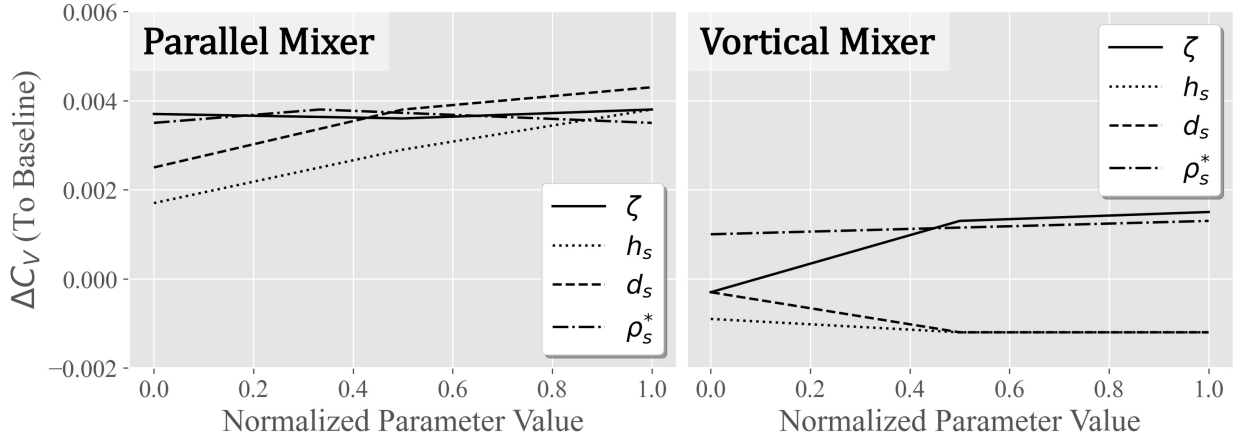
Table 7   Advanced-feature mixer case matrix.

Parallel Baseline Mixer

Varied Parameter↓	ζ	h_s	d_s	ρ_s^*
ζ	(0° 10°, 20°)	0.7	0.3	0.5
h_s	20°	(0.3, 0.5, 0.7)	0.3	0.5
d_s	20°	0.7	(0.1, 0.3, 0.5)	0.5
ρ_s^*	20°	0.7	0.3	(0.3, 0.5, 0.9)

Vortical Baseline Mixer

Varied Parameter↓	ζ	h_s	d_s	ρ_s^*
ζ	(0°, 10°, 20°)	0.6	0.1	0.3
h_s	0°	(0.5, 0.6, 0.7)	0.2	0.3
d_s	0°	0.6	(0.1, 0.2, 0.3)	0.3
ρ_s^*	20°	0.5	0.2	(0.3, 0.5, 0.9)

Aerodynamic performance was evaluated using velocity coefficient C_V, defined with Eqs.9 and 10, while ΔC_V is defined as improvement over baseline mixer performance. Plots of ΔC_V vs. each studied parameter over normalized ranges are shown in Fig. 6.

$$F_{g,i} = \dot{m}_{IN} \sqrt{R * T_{t,IN} \frac{2\gamma}{\gamma - 1} \left[1 - \left(\frac{1}{\gamma} \right)^{\frac{\gamma - 1}{\gamma}} \right]} \tag{9}$$

$$C_V = \frac{F_g}{F_{g,i}} \tag{10}$$

Fig. 6 ΔC_V vs. normalized parameters.

Features added to the parallel mixer were seen to improve performance, with increases in d_s and h_s correlating to increases in ΔC_V. The maximum increase of 0.0043, while small, is above the expected numerical error and can be considered significant. Variations in ζ and ρ_s^* were not seen to have significant effects, though these parameters were investigated at values of d_s and h_s which resulted in performance improvements. Features added to the vortical mixer were seen to have various effects, and all ΔC_V values were below or near the expected numerical error. Increasing ζ was the lone parameter to have any positive effect on ΔC_V. It is noted that parallel baseline mixer performance was calculated as $C_V = 0.954$ while vortical baseline mixer had $C_V = 0.958$, meaning more potential performance improvement was available for the parallel mixer.

The flowfield through the duct was visualized on select r-θ planes through the duct body using the following fluid properties:

- Axial vorticity magnitude $||\omega_x \hat{i}||$: Approximates streamwise vorticity, a major mechanism identified as a contributor to mixing effectiveness
- Cross-stream vorticity $\omega_{yz} = ||\omega_y \hat{j} + \omega_z \hat{k}||$: Represents gradients in the v_x field with respect to cross-stream directions, a major contributor to noise generation
- Density standard deviation $\sigma_\rho = (\oiint (\overline{\rho} - \rho)^2 dA)^{0.5}$: Inversely proportional to the mixedness of the flowstream at the given duct cross-section, where $\overline{\rho}$ is the area-average of ρ over the given r-θ plane

These quantities are not meant to determine optimal performance, but rather to simply understand the flowfield dynamics within the nozzle and direct future efforts. Figures 7 and 8 show contours of σ_ρ and $||\omega_x \hat{i}||$ for various cross-section planes over the studied range of d_s on the parallel baseline mixer, while Figs. 9 and 10 show the same over the studied range of ζ for the vortical baseline mixer. Figures 11-14 show mass flow-averaged values of σ_ρ, $||\omega_x \hat{i}||$, and ω_{yz} vs. axial location, comparing vorticity and mixedness development through the nozzle between cases for each parameter studied.

Both $||\omega_x \hat{i}||$ and ω_{yz} increase dramatically as v_x increases through the C-D nozzle section, stretching the vorticity. This correlates to a precipitous drop in σ_ρ as the increased vorticity accelerates fluid interaction between bypass and core streams, but also contributes to total pressure loss. The introduction of an additional $||\omega_x \hat{i}||$ by the scallop is evident in the parallel mixer curves shown in Fig. 13a). A small but distinct jump in $||\omega_x \hat{i}||$ is seen at different locations around the labeled x_{ss}, corresponding to each configuration's individual x_{ss} location. Looking at the x vs. σ_ρ curves in Fig. 13e), $||\omega_x \hat{i}||$ is seen to correlate to the rate of decay of σ_ρ. This additional $||\omega_x \hat{i}||$ is also evident in the contours at x_{mte} shown in Fig. 8, while the faster initial decay of σ_ρ can be seen by comparing the contours at x_{mte} and x_7 shown in Fig. 7. Despite the higher initial $||\omega_x \hat{i}||$ for $d_s = 0.3$ and 0.5, $||\omega_x \hat{i}||$ for $d_s = 0.1$ is seen to catch up and surpass the other cases beginning at x_7, corresponding to the convergent section of the nozzle. Higher ρ gradients interact with quasi-streamwise p gradients present in a C-D nozzle to generate baroclinic torque, thus contributing additional vorticity, including some in the streamwise direction. This ultimately accelerates σ_ρ decay, increasing mixedness but also generating additional ω_{yz}, which is undesirable both for aerodynamic performance, as shown in Fig. 6, and for noise suppression.

A similar conclusion can be drawn by examining Figs. 11b)/f), 10, and 9, as the introduction of a scarf cut to the vortical mixer also begins the generation of $||\omega_x \hat{i}||$ earlier in the flow mixing process. Here, Fig. 6 shows that C_V reaches a plateau at $\zeta = 10°$, likely owing to the scarf cut decreasing mixer lobe penetration into the core stream, counter-acting increases in mixing effectiveness from earlier $||\omega_x \hat{i}||$ generation. From this assessment, it is proposed that introducing $||\omega_x \hat{i}||$ into a dual-stream flow mixing process as early as possible is beneficial.

IV. Conclusion

In the present work, the concept of and specific application for lobe mixers was introduced, and precursor work on a basic parametric space for generating lobe mixers was briefly reviewed. The methodology for expanding on the basic parameter space with scarfing and scalloping features was detailed, including the geometry generation, gridding, and numerical solution elements of the process. A description of the automated nozzle construction process using the python toolset SPAND was given, along with a current state of the software's development. Results were presented from 18 advanced-feature mixer configurations, representing single-axis studies over 4 parameters on both a parallel and a vortical baseline mixer. Analysis of C_V revealed notable aerodynamic performance increases in the relations below, with no significant effects otherwise:

- Increase in d_s on the parallel mixer
- Increase in h_s on the parallel mixer
- Increase in ζ on the vortical mixer, with a plateau at $\zeta = 10°$

Flowfield analysis was given in the form of $||\omega_x\hat{i}||$, ω_{yz}, and σ_ρ development through the nozzle duct, with contour snapshots shown for select cases. The following conclusions were drawn from the findings:

- Scallop cuts were seen to introduce additional $||\omega_x\hat{i}||$
- A correlation was established between $||\omega_x\hat{i}||$ and σ_ρ decay
- Earlier introduction of $||\omega_x\hat{i}||$ leads to quicker σ_ρ decay and lower ω_{xy} at the nozzle exit, improving aerodynamic performance and reducing noise-generating v_x gradients.

Future work will continue to be directed toward development of quiet, high-performing internally-mixed plug nozzles for commercial supersonic applications. This includes further development of the SPAND toolset, introduction of discontinuous mixer features such as vortex generators, and development of a low-fidelity noise prediction metric for use with RANS solution data.

Acknowledgment

References

[1] Stitt, L. E., "Exhaust Nozzles for Propulsion Systems With Emphasis on Supersonic Cruise Aircraft," *NASA-RP-1235*, 1990. URL https://ntrs.nasa.gov/citations/19900011721.

[2] Zaman, K. Q., and Heberling, B., "A Study of Flow and Noise from Supersonic Plug Nozzles," *AIAA Paper 2021-2304*, AIAA Aviation Forum, Virtual Event, 2021. https://doi.org/10.2514/6.2021-2304.

[3] Merati, P., and Cooper, N. J., "Experimental Investigation of Flow Behavior for Scalloped and Lobed Mixers," *Advances in Mechanical Engineering*, Vol. 8, No. 9, 2016, pp. 1–17. https://doi.org/10.1177/1687814016668280.

[4] Banks, W. V., "Optimization of a Parametric Lobe Mixer for Internally Mixed Nozzles," *AIAA Paper 2022-3261*, AIAA Aviation Forum, Chicago, IL, 2022. https://doi.org/10.2514/6.2022-3261.

[5] Berton, J., Huff, D., Seidel, J., and Geiselhart, K., "Supersonic Technology Concept Aeroplanes for Environmental Studies," *AIAA Paper 2020-0263*, AIAA SciTech Forum, Orlando, FL, 2020. https://doi.org/10.2514/6.2020-0263.

[6] Menter, F. R., "Zonal Two Equation κ-ω Turbulence Models for Aerodynamic Flows," *NASA-TM-103975*, October 1993. https://doi.org/10.2514/6.1993-2906.
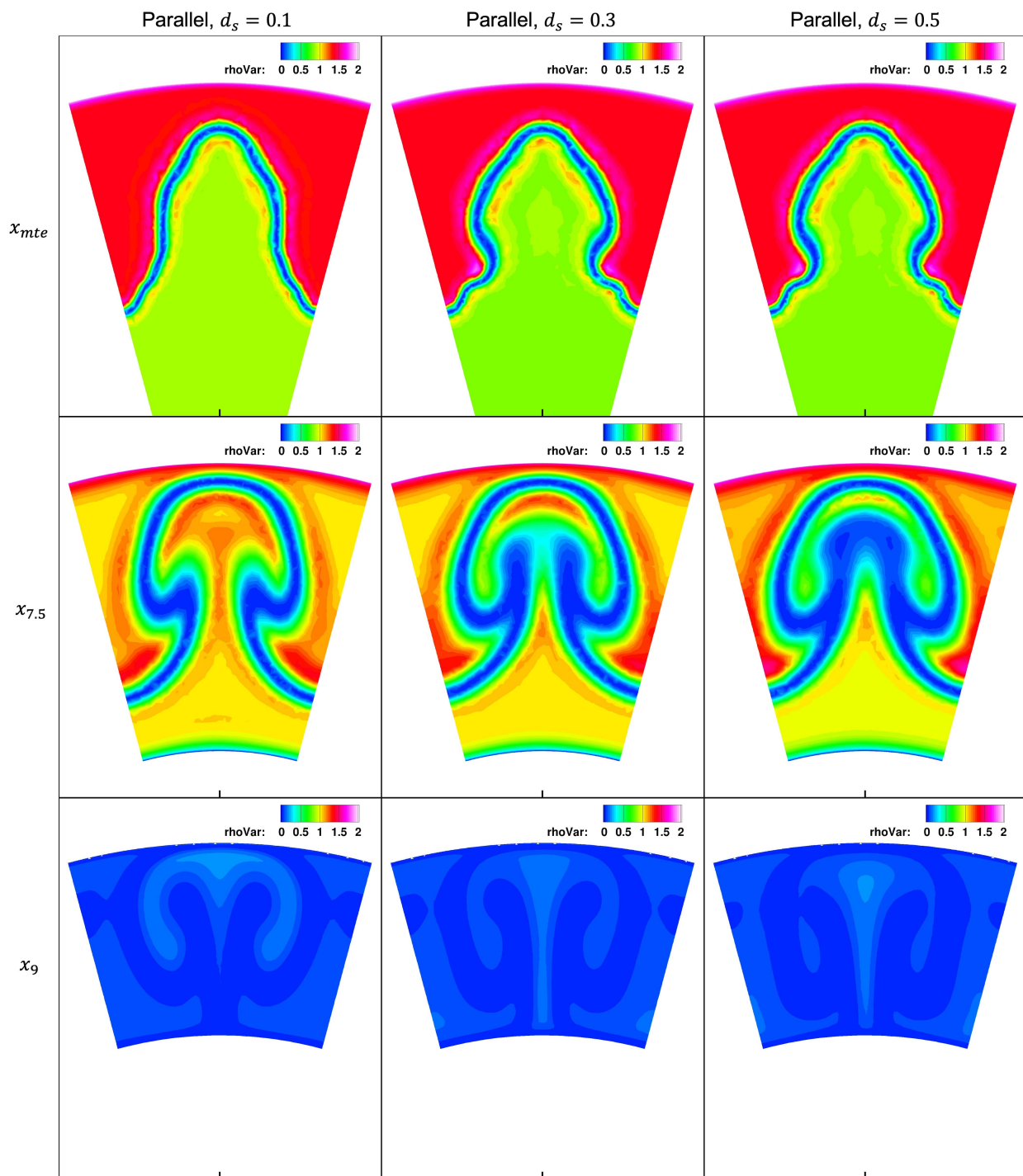
Fig. 7 Local density variation $(\overline{\rho} - \rho)^2$ through the parallel mixer nozzle for the studied range of scallop depth.
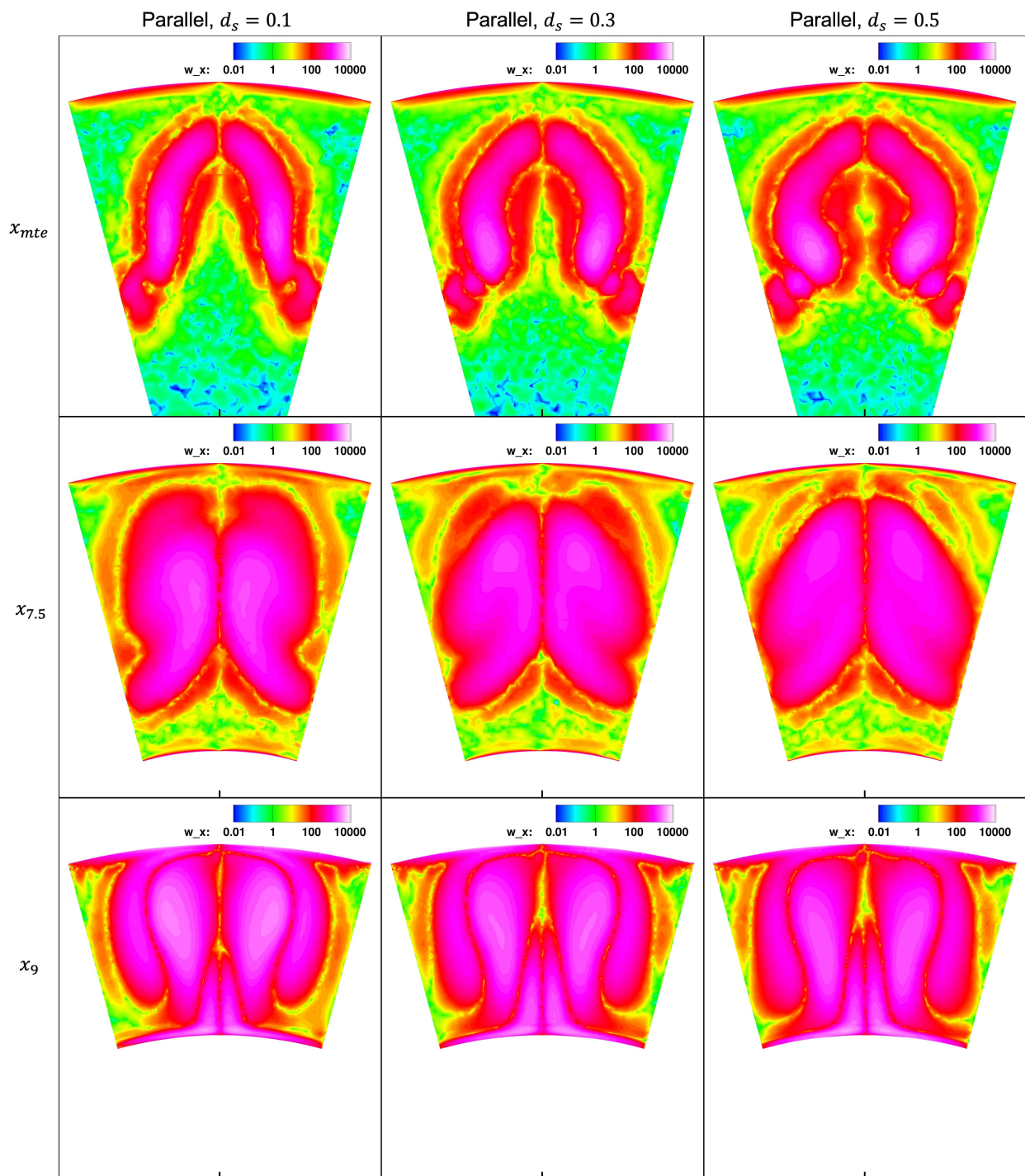
Fig. 8 Axial vorticity magnitude through the parallel mixer nozzle for the studied range of scallop depth.
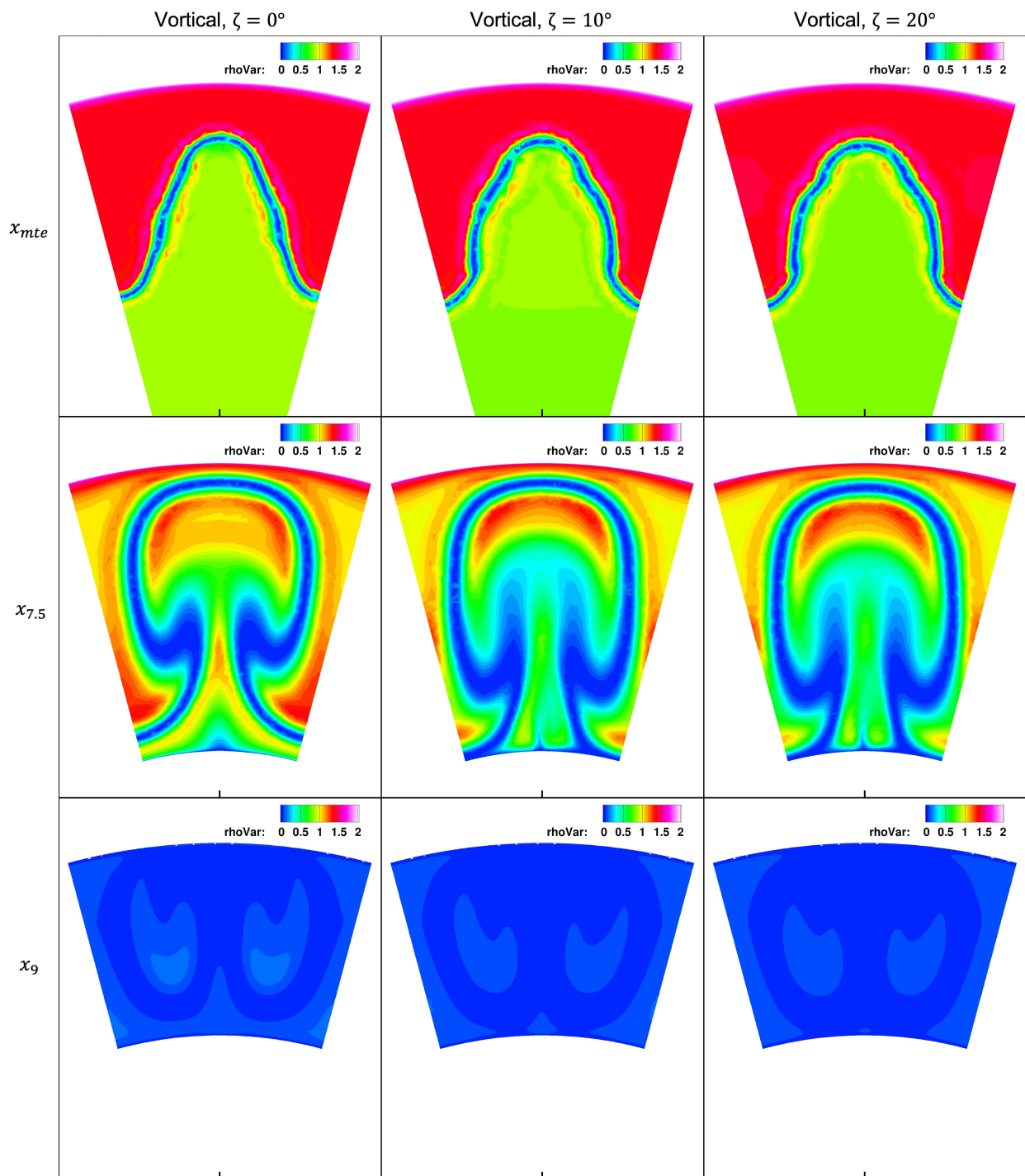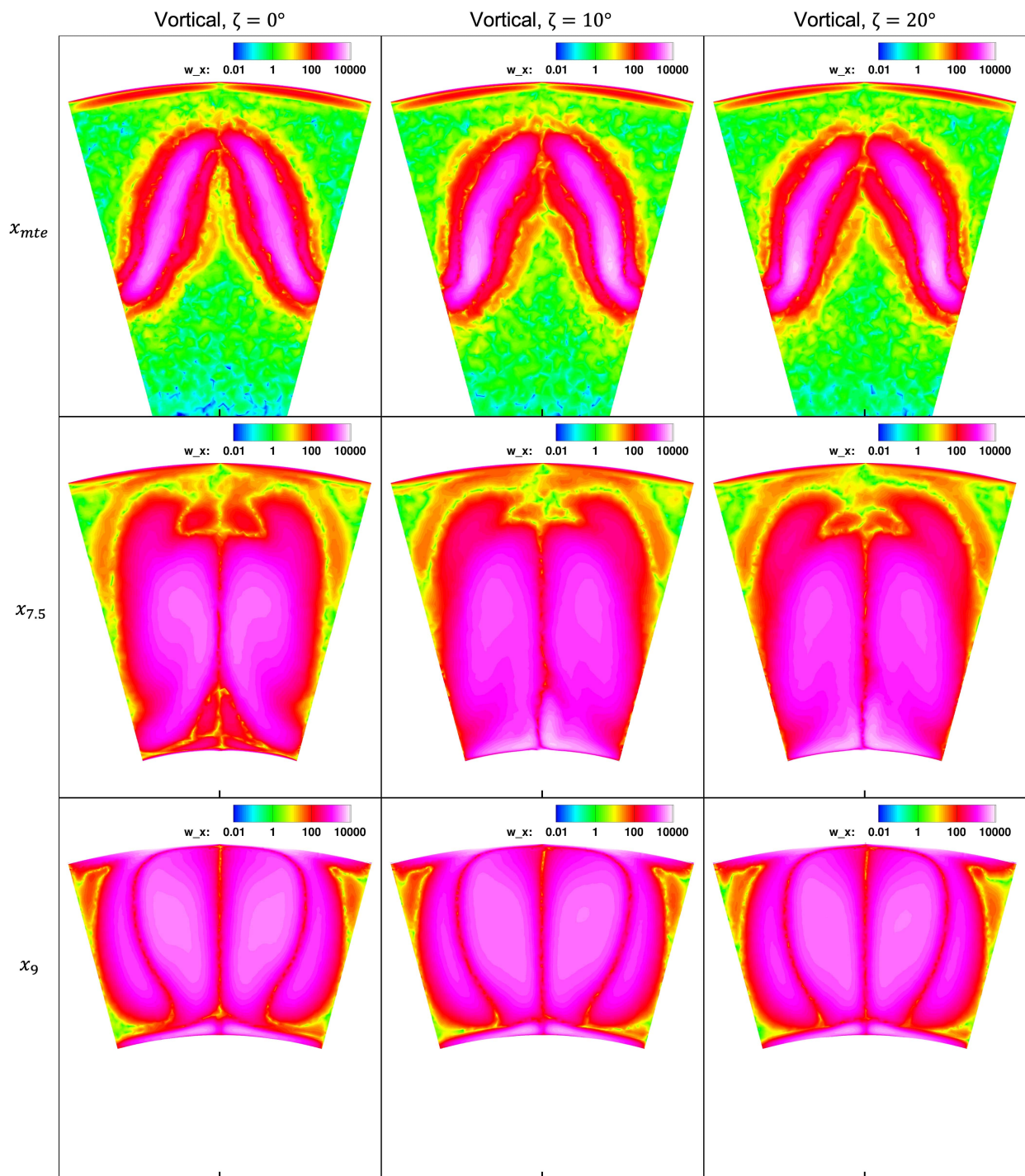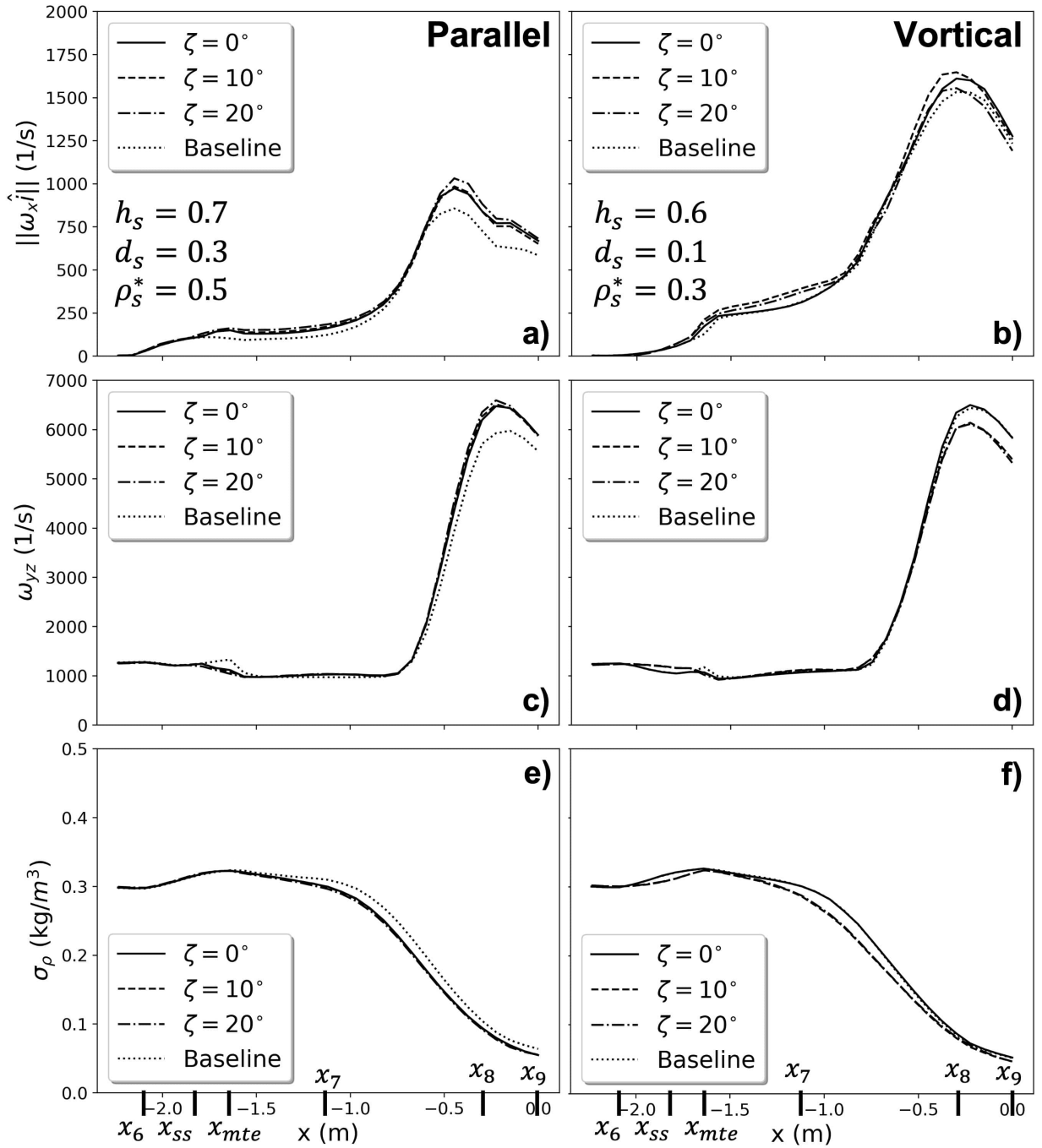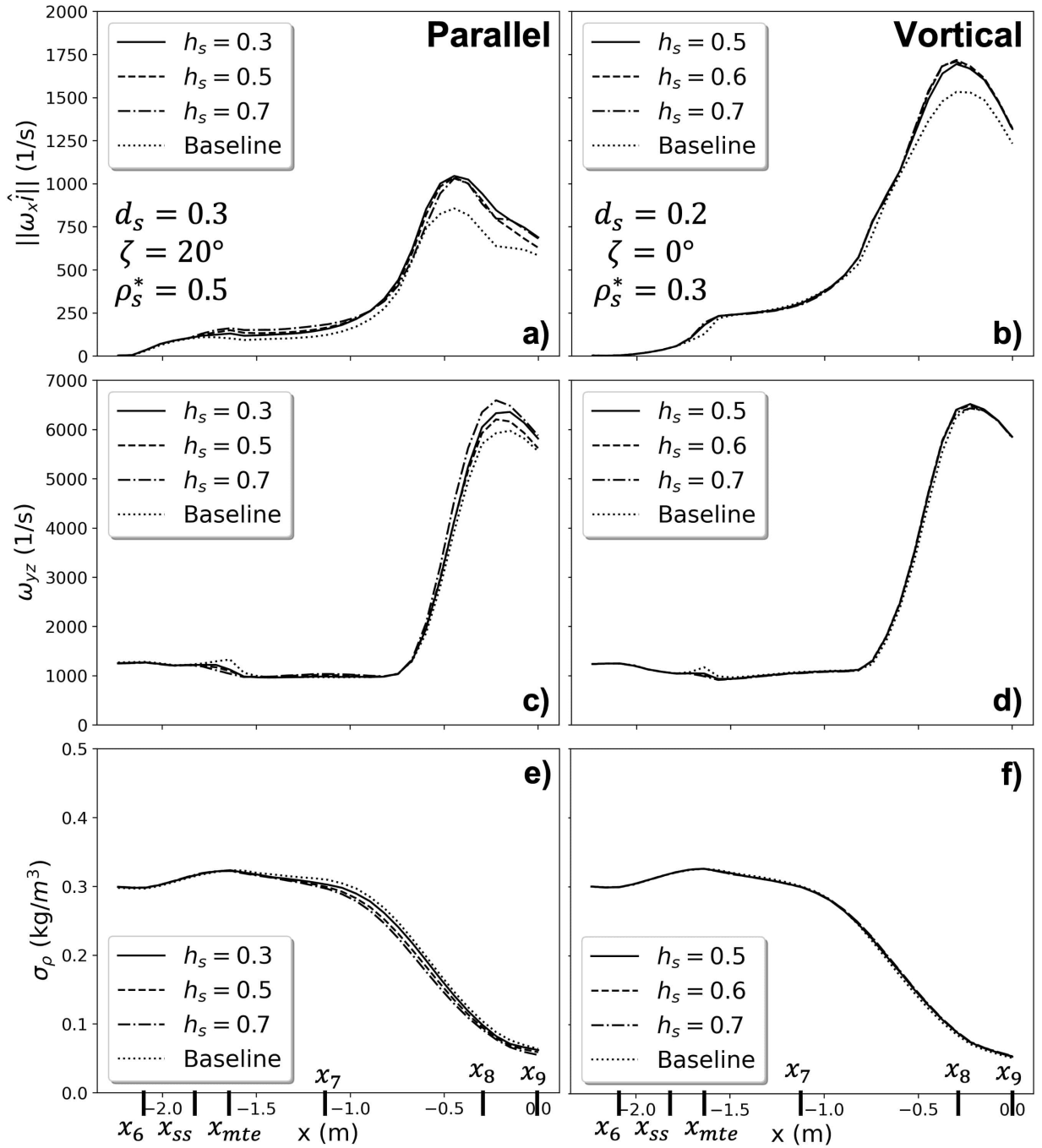
Fig. 9 Local density variation $(\overline{\rho} - \rho)^2$ through the vortical mixer nozzle for the studied range of scarf angle.

Fig. 10   Axial vorticity magnitude through the vortical mixer nozzle for the studied range of scarf angle.

Fig. 11 **Massflow-averaged vorticity and planar σ_ρ vs. x for the studied ranges of ζ.**

Fig. 12 Massflow-averaged vorticity and planar σ_ρ vs. x for the studied ranges of h_s.
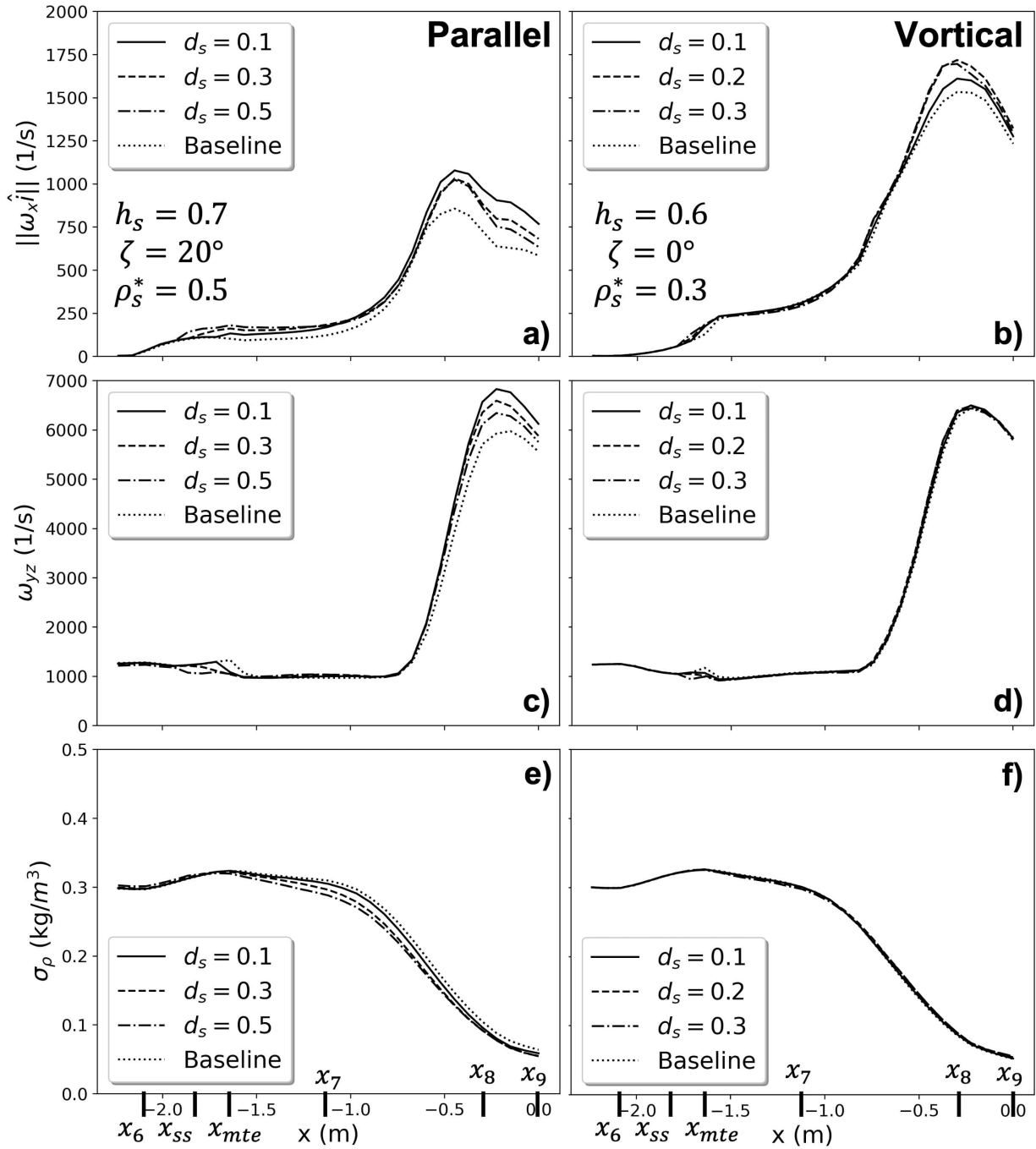
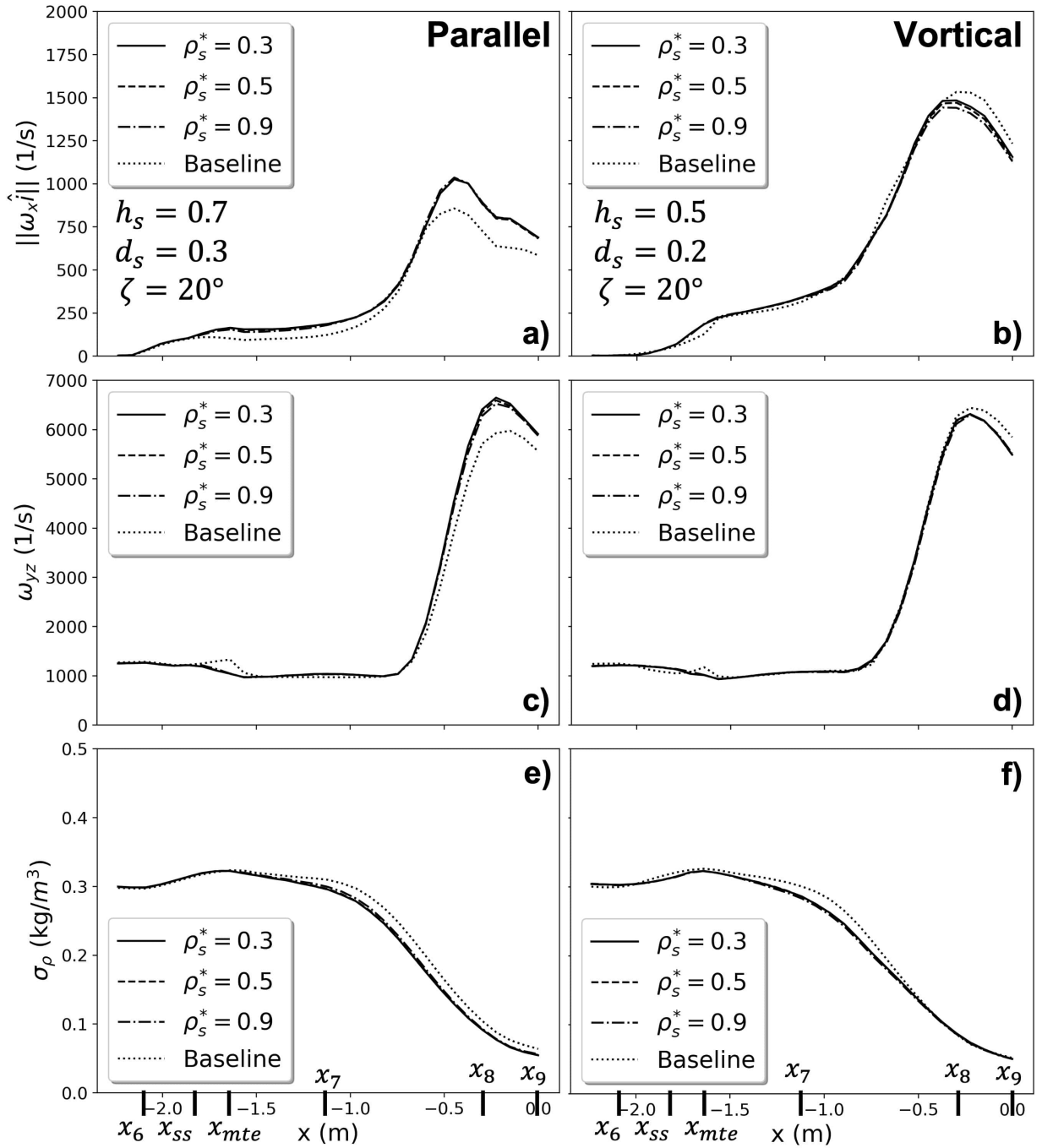Fig. 13   Massflow-averaged vorticity and planar σ_ρ vs. x for the studied ranges of d_s.

Fig. 14 **Massflow-averaged vorticity and planar σ_ρ vs. x for the studied ranges of ρ_s^*.**